Research Article

Statistical distribution of barrier heights, current conduction mechanism and voltage-dependent capacitance–frequency characteristics of Au/Fe_3O_4/n-GaN heterojunction

M. Uma[1] · M. Siva Pratap Reddy[2] · V. Rajagopal Reddy[1]

© Springer Nature Switzerland AG 2019

Abstract

This work demonstrates the modification of electrical parameters of the Au/n-GaN Schottky junction (SJ) by a thin magnetite metal (Fe_3O_4) interlayer in between the Au and n-GaN substrates. The current–voltage (*I*–*V*), voltage-dependent capacitance–frequency (*C*–*f*) and conductance–frequency (*G*–*f*) characteristics of the Au/Fe_3O_4/n-GaN heterojunction (HJ) are systematically studied. Using statistical analysis, the mean barrier heights and ideality factors are found to be 0.70 eV and 1.62 for the SJ and 0.84 eV and 1.87 for the HJ, respectively. It is noticed that the mean barrier height of Au/Fe_3O_4/n-GaN HJ increases as compared that of the Au/n-GaN SJ, indicating the Fe_3O_4 interlayer modified the barrier height. The SJ revealed a transition from Poole–Frenkel emission at low voltages to Schottky emission at high voltages. However, the HJ exhibited Schottky emission over whole voltage range. It is observed that the higher values of capacitance decrease at low frequencies that are attributed to the excess capacitance resulting from the interface states in equilibrium with the n-GaN which could respond the ac signal. The interface states density (N_{SS}) and relaxation time (τ) of the Au/Fe_3O_4/n-GaN HJ are estimated from *C*–*f* plots, respectively. The N_{SS} reveals that the interface states decrease with voltage from the bottom of the conduction band toward the mid-gap.

Keywords Fe_3O_4 interlayer · n-GaN substrate · Voltage-dependent *C*–*f* and *G*–*f* properties · Interface state density · Relaxation time

1 Introduction

Gallium nitride (GaN) has grown to be very promising semiconductor material for the development of optoelectronic, high-power and high-frequency devices [1, 2]. In general, GaN-based materials attracted in small spin–orbit coupling due to its wide band gap; this is splendid for spintronic applications [3, 4]. Specifically, GaN-based spintronic devices would be very effective than GaAs-based devices for the cause of the long spin transport length in this material [5–7]. In fact, the spin transistor contains one ferromagnetic metal contact that works as a spin injector while the other one acts as a spin detector. Very interestingly, these issues could be closely related to recent works in semiconductor spintronics [8]. From this point of view, it can be concluded that every semiconductor spintronic device needs ferromagnetic metal contact in an effective way for feasible manufacturing purpose. Ferromagnetic metal-based schemes have been widely examined for the fabrication of Schottky contacts on semiconductors [9–13]. For example, Van Erve et al. [9] demonstrated that the Fe/AlGaAs interface showed highly efficient spin injection. Garrido et al. [10] reported the electrical properties of Fe/GaN Schottky barrier contacts and showed the barrier contact satisfies the spin injection experiments. Kumar et al. [11] fabricated Fe Schottky contacts on GaN and

✉ M. Siva Pratap Reddy, dr.mspreddy@gmail.com; ✉ V. Rajagopal Reddy, reddy_vrg@rediffmail.com | [1]Department of Physics, Sri Venkateswara University, Tirupati 517502, India. [2]School of Electronics Engineering, Kyungpook National University, Daegu 41566, South Korea.

SN Applied Sciences (2019) 1:428 | https://doi.org/10.1007/s42452-019-0430-7

Received: 22 January 2019 / Accepted: 29 March 2019 / Published online: 8 April 2019

investigated the temperature-dependent *I–V* characteristics in a wide range of 100–300 K and found an inhomogeneous behavior at the Fe and GaN interface, which makes spin relaxation time in GaN for spintronic applications. Janardhanam et al. [12] fabricated the $Ni_{0.8}Fe_{0.2}$/n-type GaN Schottky diodes and reported the barrier height and ideality factor as a function of temperature. Yang et al. [13] demonstrated the current–voltage (*I–V*) characteristics of Fe_3O_4/Nb-doped $SrTiO_3$ (Nb: STO) and Fe_3O_4/ZnO junctions that were prepared by pulsed laser deposition. They showed that the rectifying behavior of Fe_3O_4/Nb: STO junction was better than that of the Fe_3O_4/ZnO junctions.

Based on the above review, in this work, it is proposed to fabricate and characterize the Au/Fe_3O_4/n-GaN heterostructure (HJ) with a magnetite interlayer and analyzed by current–voltage (*I–V*) and capacitance–frequency (*C–f*) measurements. Some researchers have reported the using of ferromagnetic metals as contact or an interfacial layer between the metal and semiconductor (MS) junctions such as Ni, Co, Fe, magnetite (Fe_3O_4), nickel–iron alloy (NiFe) and permalloy ($Ni_{0.8}Fe_{0.2}$) [14–16]. In the present work, magnetite (Fe_3O_4) is selected since it is used in a variety of applications such as catalysis, bio-processing, audio and videotape, high-density digital recording, magnetic fluids and information and energy storage, including microwave devices, magneto-optics devices, sensors and high-frequency applications [17–22]. Also, Fe_3O_4 may be used as ferromagnetic material for electrodes in magnetic tunnel junctions (MTJ) [23]. Further, Fe_3O_4 is non-toxic and biocompatible. Due to exceptional properties of Fe_3O_4 material, in this work, the Au/Fe_3O_4/n-GaN heterojunction (HJ) is fabricated with a Fe_3O_4 interlayer in between the metal and n-GaN, the electronic parameters such as barrier height (Φ_b) and ideality factor (*n*) are examined, and these electronic parameters are compared with the conventional Au/n-GaN Schottky junction (SJ). The statistical distribution analysis is applied to obtain the mean values barrier height and ideality factors of SJ and HJ using Gaussian distribution function. Afterward, the capacitance–frequency (*C–f*) and conductance–frequency (*G–f*) characteristics of the Au/Fe_3O_4/n-GaN HJ are measured in the frequency range of 1 kHz to 1 MHz with different applied biases at room temperature. Finally, the interface state density distribution and relaxation time of the Au/Fe_3O_4/n-GaN HJ are estimated and discussed.

2 Experimental details

GaN (Si-doped) wafers with 2 µm thickness grown on c-plane Al_2O_3 (0001) sapphire substrate using metal organic chemical vapor deposition method and carrier concentration of about 4.07×10^{17} cm^{-3} were used in this work. Prior to deposition of magnetite (Fe_3O_4), the n-type GaN samples were ultrasonically cleaned with warm trichloroethylene followed by acetone and methanol for 5 min each step. The samples were then dipped into buffered oxide etch (BOE) solution for 10 min to remove the native/surface oxide layer and immersed in deionized (DI) water. After this procedure, the wafer was dried with N_2 atmosphere. In order to make both ohmic and Schottky electrodes, standard photolithography and lift-off approaches were used. To make ohmic contacts, Ti and Al metals were deposited sequentially with thickness of 25 and 100 nm by electron beam (e-beam) evaporation approach. Then, the contacts were immediately annealed at 750 °C in N_2 ambient for 1 min using a rapid thermal annealing system and the defined electrodes were dipped into a BOE solution for 30 s. Next, the magnetite (Fe_3O_4) was deposited using an electron beam method on cleaned n-type GaN surface followed by 30 nm thickness gold as Schottky contact. The circular Schottky electrode area was 3.14×10^{-4} cm^2. The current–voltage (*I–V*) characteristics were carried out using a Keithley source unit 2400. In addition, the voltage-controlled capacitance–frequency (*C–f*) and conductance–frequency (*G–f*) characteristics were evaluated using a phase sensitive multimeter unit PSM 1700.

3 Results and discussion

In order to confirm the heterojunction formation, transmission electron microscopy (TEM) measurement is employed. Figure 1a shows the cross-sectional bright-field TEM image obtained from Fe_3O_4/n-GaN heterojunction. Figure 1a demonstrates the excellent feature of the interface between Fe_3O_4 and n-GaN, and it is observed crystalline of the Fe_3O_4 on n-type GaN. To determine the average values of barrier heights and ideality factors, we fabricated ten diodes of the Au/n-GaN Schottky junction (SJ) and Au/Fe_3O_4/n-GaN heterojunction (HJ) that are prepared identically on the same wafer. Figure 1 exhibits the *I–V* characteristics of the foremost samples of the SJ and HJ. Both the SJ and HJ exhibit a good rectification behavior with the reverse leakage currents of 1.37×10^{-6} A for the SJ and 3.26×10^{-8} A at −1 V for the HJ. It is noted that the leakage current of HJ reduces almost two orders as compared to the SJ, indicating the formation of Fe_3O_4 interlayer enforced the improved electrical properties of the HJ. The series resistance (R_S) is an important factor for the device fabrication. The R_S of the both junctions is determined from *I–V* characteristics (Fig. 1), and the respective values are 16.42 Ω and 22.54 Ω for the SJ and HJ, respectively. It is noted that the junction with Fe_3O_4 interlayer results in a considerable increase in R_S, indicating that Fe_3O_4 interlayer plays a key role for the formation of

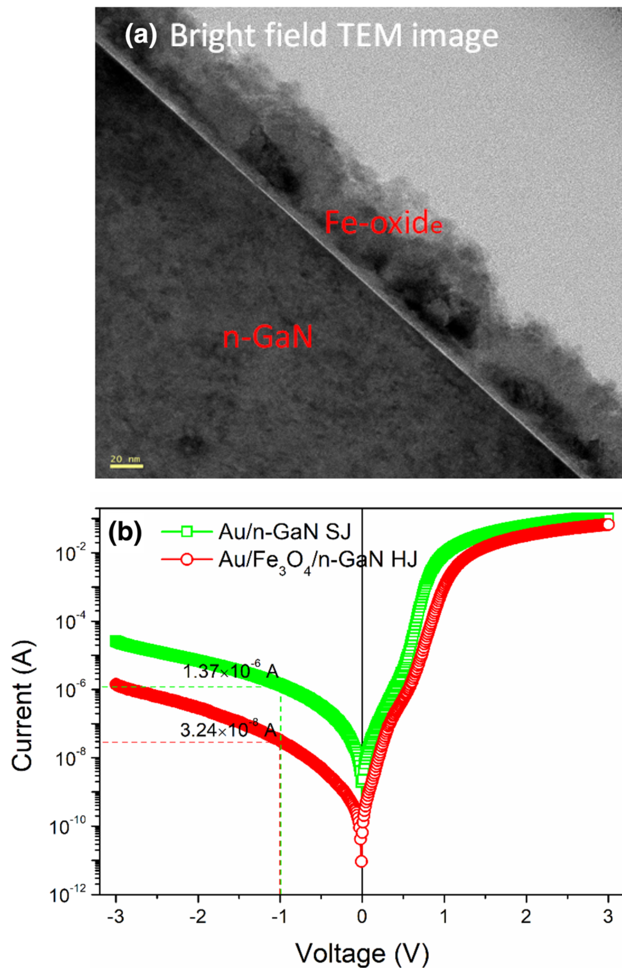

Fig. 1 **a** Bright-field TEM image of the Fe_3O_4/n-GaN junction and **b** semi-log *I–V* characteristics of the Au/n-GaN SJ and Au/Fe_3O_4/n-GaN HJ in the forward and reverse bias

barrier in between the metal and semiconductor. The current transport in a Schottky diode with an interlayer at forward bias ($qV > 3kT$) is especially explained via thermionic emission phenomena as [24, 25]

$$I = I_s\left[e^{\left(\frac{qV}{nkT}\right)} - 1\right] \tag{1}$$

$$I_S = AA^*\theta_p T^2 e^{\left(\frac{-q\Phi_{bh,0}}{kT}\right)} \tag{2}$$

where q is the charge of electron, V is the applied voltage, n is the ideality factor, k is the Boltzmann constant, T is the temperature, A is the contact area, $\Phi_{bh,0}$ is the zero bias barrier height and θ_p is the transmission coefficient over the interlayer and is found to be [26]

$$\theta_p = \exp\left(-\frac{4\pi\delta}{h}(2m^*\chi)^{1/2}\right) = \exp\left(-a\delta(\chi)^{1/2}\right) \tag{3}$$

where $a = (4\pi/h)(2m^*)^{1/2}$ is a constant dependent on the electron mass, $m^* = 0.22\, m_0$, δ is the thickness of the interlayer and χ is the mean tunneling barrier height affected by the thin interlayer. If the interlayer is very thin, the value should be $\theta_p \approx 1$. The barrier height from the logarithmic *I–V* characteristics is extracted using the extrapolation of I_S values by the following relation:

$$\Phi_{bh} = q\left(\frac{1}{kT}\right)\ln\left(\frac{AA^*T^2}{I_S}\right) \tag{4}$$

Combining Eqs. (2)–(4), we get [26]

$$\Phi_{bh} = \Phi_{bh,0} + akT\delta\chi^{1/2}. \tag{5}$$

Based on the logarithmic *I–V* data, the slope gives the ideality factor, *n*, values and the values extracted for ten diodes are in the range of 1.51–1.74 and 1.69–1.93 for the Au/n-GaN SJ and Au/Fe_3O_4/n-GaN HJ, respectively. The obtained values of ideality factor are higher than one for both the junctions. These high values may be due to the image force lowering, interface states existence at the interface, non-uniform interlayer formation between the metal and semiconductor, and barrier inhomogeneities [27–29]. The barrier heights are evaluated for ten fabricated diodes and the estimated effective Φ_{bh} ranging from 0.64 to 0.74 eV and 0.74–0.86 eV for the Au/n-GaN SJ and Au/Fe_3O_4/n-GaN HJ, respectively.

Basically, the ideality factor and barrier height values are changed from junction to junction even though the junctions are fabricated with same conditions. In fact, analysis shows that the barrier height between the metal and semiconductor effectively depends on the applied bias excluding the image force effect for the ideal diodes. Therefore, it is important to analyze results with average ideality factor and barrier height values using statistical distribution analysis. Figures 2 and 3 show the statistical distribution, and box and whisker plots of the ideality factor and barrier height values obtained from the *I–V* data and fitted by Gaussian distribution function for ten Au/n-GaN SJ (Figs. 2a, c, 3a, c) and Au/Fe_3O_4/n-GaN HJ (Figs. 2b, c, 3b, c). The average ideality factor values of 1.62 and 1.87 with normalization deviation of 0.09 and 0.08 for the Au/n-GaN SJ and Au/Fe_3O_4/n-GaN HJ, respectively, are obtained from the statistical analysis (Fig. 2a, c). From Fig. 3a, c, the statistical analysis provides average barrier height values of 0.70 eV and 0.84 eV with normalization deviation of 0.02 eV and 0.08 eV for the Au/n-GaN SJ and Au/Fe_3O_4/n-GaN HJ, respectively. The barrier height estimated for the Au/Fe_3O_4/n-GaN HJ compared with that of the reported barrier height values obtained for the other devices in the literature, for instance, is 0.72 eV for Al/Fe_3O_4/p-Si junction [30], 0.88 eV for Au/Fe_3O_4/p-Si Schottky contacts [31], 0.82 eV for Au/CZTS/n-GaN HJ [32], 0.98 eV for Au/Gd_2O_3/n-GaN HJ [33], 0.94 eV Au/ZrO_2/n-GaN MIS junction

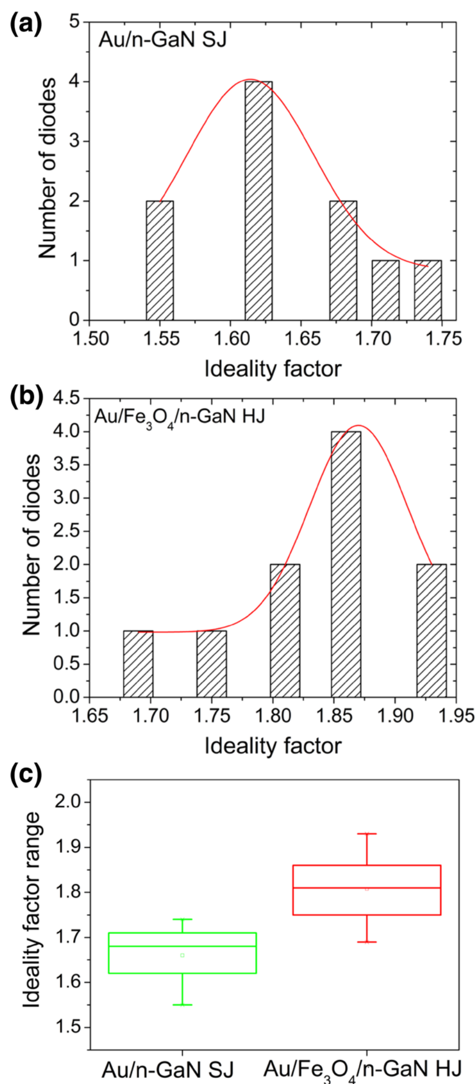

Fig. 2 Gaussian distribution of ideality factors for the **a** Au/n-GaN SJ and **b** Au/Fe_3O_4/n-GaN HJ, and **c** box–whisker plot of ideality factors for the Au/n-GaN SJ and Au/Fe_3O_4/n-GaN HJ

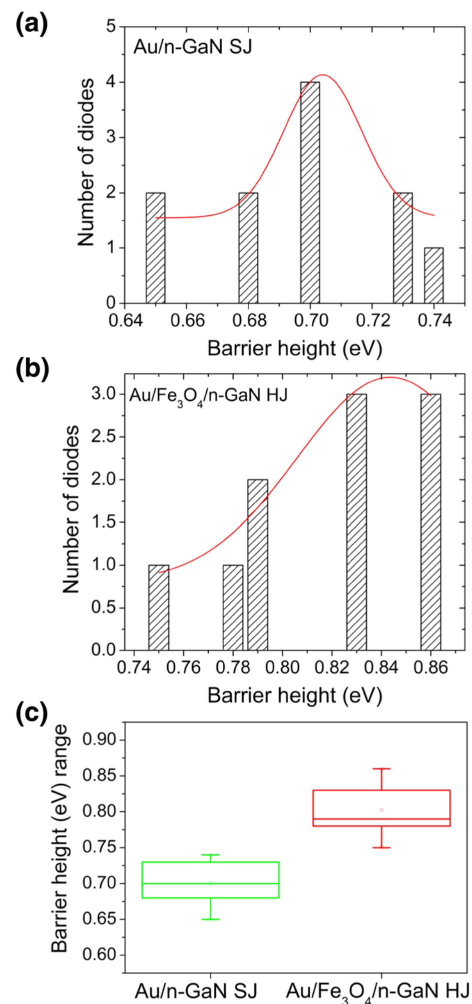

Fig. 3 Gaussian distribution of barrier heights for the **a** Au/n-GaN SJ and **b** Au/Fe_3O_4/n-GaN HJ, and **c** box–whisker of barrier heights for the Au/n-GaN SJ and Au/Fe_3O_4/n-GaN HJ

[34]. It is noted that the average barrier height difference between Au/n-GaN SJ and Au/Fe_3O_4/n-GaN HJ is 0.14 eV. This may be the cause of occurrence of the interlayer between the Au and n-GaN, which plays as a physical barrier. The potential change in barrier height for the Au/Fe_3O_4/n-GaN HJ could be explained on the basis of surface energy band bending between the interlayer and III–V semiconductors. In addition, the change may also create a native barrier lowering effect caused by field emission at metallic diffusion spikes with confined radii of curvature [29]. The deviation of the barrier height of Au/Fe_3O_4/n-GaN HJ is more than the Au/n-GaN SJ, due to the excess deviation in thickness of the Fe_3O_4 layer developed on the GaN substrate.

In order to prove that the increase in barrier height and decrease in current in the Au/Fe_3O_4/n-GaN HJ should be explained using tunneling probability $\exp(-\alpha\delta(\chi)^{1/2})$ or on the interlayer thickness. Figure 1 shows the current in both directions (forward and reverse) in the Au/Fe_3O_4/n-GaN HJ is reduced compared to the Au/n-GaN SJ due to the existence of interlayer, and the linear intercept (I_S) value of the forward bias current is lower than that without interlayer one (SJ). Moreover, an average ideality factor value (1.87) shows that the structure conforms metal/interlayer/III–V semiconductor (MIS) structure instead of the ideal SJ. The tunneling barrier height is obtained as $\chi = 0.14$ eV for the Au/Fe_3O_4/n-GaN HJ using Eq. (5). According to Card and Rhoderick [35], the increase in barrier height was influenced by interlayer which is due to the tunneling in both n- and p-type semiconductors.

The reverse leakage current conduction mechanism of the SJ and HJ was analyzed by using Poole–Frenkel emission (PFE) and Schottky emission (SE) models from the plot of $\ln(I_{rev})$ versus voltage $(V_{rev})^{1/2}$, as shown in Fig. 4. The reverse leakage current is dominated by Poole–Frenkel emission as follows [1, 36, 37]:

$$I_{rev} = I_0 \exp\left(\frac{b_{PF}\sqrt{V_{rev}}}{kT\sqrt{\delta}}\right) \tag{6}$$

and the lowering the Schottky barrier is [1, 37, 38]

$$I_{rev} = AT^2A^* \exp\left(\frac{-\Phi_b}{kT}\right) \exp\left(\frac{b_{SC}\sqrt{V_{rev}}}{kT\sqrt{\delta}}\right) \tag{7}$$

where δ is the thickness of the film and b_{PFE} and b_{SE} are the field lowering coefficients of PFE and SE, respectively. The theoretical value of the b_{PFE} and b_{SE} can be described as

$$b_{PFE} = 2b_{SE} = \left(\frac{q^3}{\pi\varepsilon_0\varepsilon_r}\right)^{1/2} \tag{8}$$

From Eq. (8), the calculated theoretical field lowering coefficient values, b_{PFE} and b_{SE}, and measured slope values for ten Au/n-GaN SJ and Au/Fe_3O_4/n-GaN HJ diodes are represented in Table 1. As shown in Table 1, the experimental slope values are close to the theoretical values of PFE at lower bias region and SE at higher bias region for the SJ, whereas slope value is closely matched with the theoretical value of PFE for the HJ. Hence, the current conduction of the Au/n-GaN SJ is affected by Poole–Frenkel emission at lower bias (region I) below 0.7 V and by Schottky emission at high bias (region II) above 0.7 V, whereas the Au/Fe_3O_4/n-GaN HJ follows Poole–Frenkel emission over the entire voltage range. Specifically, Poole–Frenkel emission is closely related to the tunneling of carriers and also associated with wide distribution of traps in the band gap of dielectric material. In addition, the traps act as impurities and/or structural defects may cause the trapping/detrapping carriers affecting the device performance. However, the Schottky emission is directly responsible for the conduction through the contact interface rather than from bulk material.

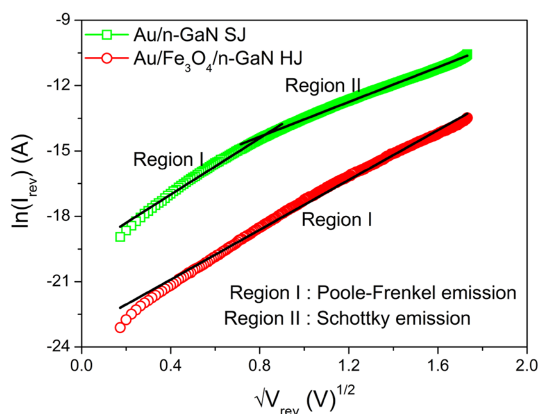

Fig. 4 Plots of $\ln(I_{rev})$ versus $\sqrt{V}$ of Au/n-GaN SJ and Au/Fe_3O_4/n-GaN HJ obtained from the reverse leakage currents

In general, a good way to extract information on Schottky diodes, capacitance measurement is one of the best nondestructive methods. Based on the theory, it is found that the measured capacitance is larger than the space charge capacitance in the forward bias of some diodes. The difference between the measured capacitance and the space charge is called the excess capacitance and is ascribed to interface states. In fact, this interface states were created by the interdiffusion of atoms, dislocations or discontinuities in crystal lattices or dangling bonds in crystal which is close to the metal/III–V semiconductor interface. The interface states capacitance is a function of the frequency and forward bias current [39–41]. Figure 5 shows the room temperature voltage-dependent capacitance–frequency (*C*–*f*) characteristics of the Au/Fe_3O_4/n-GaN HJ in the voltage range from 0.0 to 0.6 V with steps of 0.1 V. At depletion region, the measured capacitance decreases with frequency for all voltages (Fig. 5). It is noticed that the high value of measured capacitance located at lower frequencies is attributed to excess capacitance arising from the interface states that are equilibrium with III–V semiconductor (n-GaN) and respond to the ac signal [42–45]. These behaviors direct to continuous distribution of interface states, which play a key role to reduce of the response of the interface states to the applied voltage [46, 47]. Figure 6 displays the measured

Table 1 Theoretical and experimental slope values of Poole–Frenkel emission and Schottky emission for ten Au/n-GaN SJ and Au/Fe_3O_4/n-GaN HJ diodes

Sample	Poole–Frenkel emission		Schottky emission	
	Theoretical	Experimental	Theoretical	Experimental
	($\times 10^{-5}$ eVm$^{1/2}$ V$^{-1/2}$)		($\times 10^{-5}$ eVm$^{1/2}$ V$^{-1/2}$)	
Au/n-GaN SJ	2.44	(2.09 ± 0.05) (region I)	1.22	(1.3 ± 0.05) (region II)
Au/Fe_3O_4/n-GaN HJ	1.42	(1.68 ± 0.05) (region I)	0.71	–

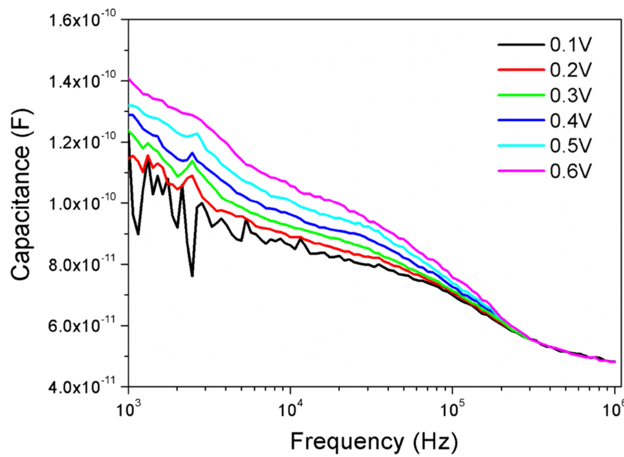

Fig. 5 Measured voltage-dependent *C–f* characteristics of the Au/Fe_3O_4/n-GaN HJ in the range of 0.0–0.6 V in steps of 0.1 V

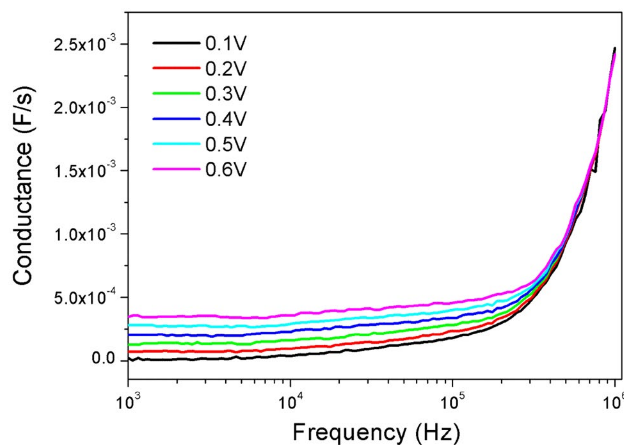

Fig. 6 Measured voltage-dependent *G–f* characteristics of the Au/Fe_3O_4/n-GaN HJ in the range of 0.0–0.6 V in steps of 0.1 V

voltage-dependent conductance–frequency (*G–f*) characteristics of the Au/Fe_3O_4/n-GaN HJ in the voltage range from 0.0 to 0.6 V with steps of 0.1 V. The *G–f* data reveal that the conductance has nearly constant value at low frequency regime (10^3–10^5 Hz), and afterward, the conductance suddenly increases with an increasing frequency for different voltages.

The interface state density for the Au/Fe_3O_4/n-GaN HJ can be calculated from the capacitance method using the Schottky capacitance spectroscopy (SCS) measurement. Using SCS approach, one can determine the accurate values of interface state capacitance as a function of frequency [48, 49]. The capacitance due to interface states that are in equilibrium with the semiconductor does not add at sufficiently high frequencies, since the interface charge at the interface states cannot respond to the ac signal. At this moment, the Schottky diode has only the space charge capacitance. The voltage-dependent *C–f* characteristics approximately equal to the sum of space charge capacitance (C_{SC}) and the interface capacitance (C_{SS}) at low frequencies. The capacitance of the Schottky diodes depends on the frequency, and it can be expressed as [42, 48]

$$C = C_{SC} + C_{SS} \text{ (i.e., lower frequency regime)} \tag{9}$$

$$C \approx C_{SC} \text{ (i.e., higher frequency regime)} \tag{10}$$

The interface state capacitance is expressed as [42]

$$C_{SS} = \left(AqN_{SS}\right)\left(\frac{\arctan(\omega\tau)}{\omega\tau}\right) \tag{11}$$

where $\omega = 2\pi f$ is the radial frequency and τ is the time constant of the interface states and it can be expressed as

$$\tau = \frac{e^{qV_d/kT}}{\sigma V_{th} N_d} \tag{12}$$

where V_d is the voltage across the diode, σ is the cross section of interface states, V_{th} is the thermal voltage and N_d is the doping concentration. The interface state density for lower value of $\omega\tau$ should be [42, 50]

$$N_{SS} = \frac{1}{qA}\left(C_{SS}\right) \tag{13}$$

where C_{SS} is found from the vertical axis intercepts of *C–f* plots. In n-type semiconductor, the distribution energy (E_{SS}) of the interface states with respect to the bottom of the conduction band (E_C) at the surface of the semiconductor and is expressed as [50]

$$E_C - E_{SS} = q\left(\Phi_b - V\right) \tag{14}$$

The total density of interface states (N_{SS}) is obtained by the experimental *C–f* measurement of the Au/Fe_3O_4/n-GaN HJ. The N_{SS} can be extracted for each applied voltage directly from the ordinate of the plateau region of *C–f* plots. Consequently, Eq. (11) is fitted to the experimental values of *C–f* to calculate relaxation time (τ) of the interface states. To extract the voltage-dependent N_{SS} and τ values, the fitting procedure is repeated for different voltages. The dependence of N_{SS} and τ on the different voltages is converted to function of E_{SS} by using Eq. (14). Figure 7 shows the experimental N_{SS} and τ versus E_C–E_{SS} plots at room temperature. It is noticed that the N_{SS} achieved from the capacitance approach has an exponential increase with voltage from the mid-gap toward the bottom of the conduction band and values are ranging from 2.32×10^{12} eV^{-1} cm^{-2} at E_C-0.23 eV to 2.38×10^{12} eV^{-1} cm^{-2} at E_C-0.73 eV, respectively. The Fermi level fix based on these trap levels at a given bias and actual electron density will be at the interface of interlayer/GaN, which results the capture rate of the related trap levels. In fact, this capture and

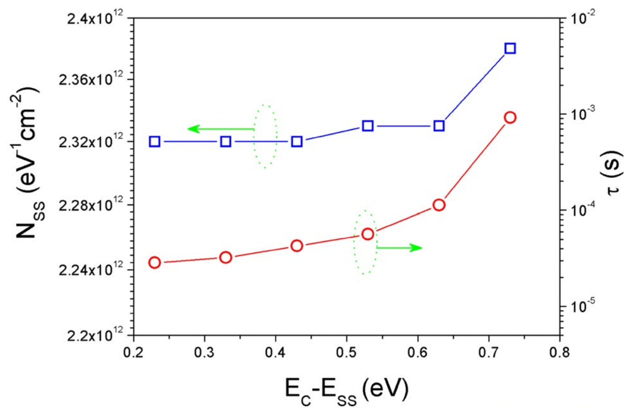

Fig. 7 Plots of relaxation time (τ) versus E_C–E_{SS} and interface state density (N_{SS}) versus E_C–E_{SS} for the Au/Fe_3O_4/n-GaN HJ

emission arise from traps located within a few values of *kT*/*q* above and below the Fermi level. If the frequency is considerably change from the capture rate, losses are minimized for the reason that trap levels either do not respond with different frequencies. The N_{SS} estimated in this work is comparable with that reported N_{SS} in the literature. For example, Bulbul et al. [51] have reported the N_{SS} ranging from 2×10^{10} to 5×10^{12} eV^{-1} cm^{-2} for the Au/$Bi_4Ti_3O_{12}$/SiO_2/n-Si (MFIS) structures. Erdogan and Gullu [52] demonstrated that the N_{SS} for the Au/Cr_2O_3/*p*-Si device varied from 2.90×10^{13} to 8.45×10^{12} eV^{-1} cm^{-2}. Rajagopal Reddy et al. [53] have reported the N_{SS} varied from 2.743×10^{12} to 5.614×10^{11} eV^{-1} cm^{-2} for the Au/NiO/n-GaN heterojunction. Venkata Prasad et al. [54] showed that the N_{SS} for the Au/Y_2O_3/n-GaN MIS diode varied from 6.268×10^{12} to 2.094×10^{12} eV^{-1} cm^{-2}. Manjunath et al. [55] demonstrated the N_{SS} being varied from 9.753×10^{12} to 1.990×10^{11} eV^{-1} cm^{-2} for the Au/Sm_2O_3/n-GaN MIS structure. The estimated interface state density of the Au/Fe_3O_4/n-GaN heterojunction is in a good agreement with that of the reported values. In addition, Fig. 7 shows the relaxation time (τ) values show a slow exponential increase from the top of the valance band with regard to the mid-gap and the values are 2.85×10^{-5} s at E_C-0.23 eV and 9.21×10^{-4} s at E_C-0.73 eV, respectively. So, it is observed that the obtained τ values are clearly voltage dependent at room temperature measurements.

4 Conclusions

In summary, the statistical distribution barrier heights, reverse current conduction mechanism, voltage-dependent capacitance–frequency (*C*–*f*) and conductance–frequency (*G*–*f*) characteristics of the Au/Fe_3O_4/n-GaN heterojunction (HJ) are investigated. The average barrier heights and ideality factors are extracted by statistical analysis from *I*–*V* characteristics, and the values are 0.70 eV and 1.62 for the Au/n-GaN Schottky junction (SJ) and 0.84 eV and 1.87 for the Au/Fe_3O_4/n-GaN heterojunction, respectively. Results show that the barrier height for the HJ is enhanced with 0.14 eV than the SJ, which is attributed to the insertion of the interlayer (Fe_3O_4) between the Au and n-GaN substrates. Observations showed a transition from Poole–Frenkel emission at lower voltage range to Schottky emission at higher voltage range for the SJ, while the HJ exhibited Poole–Frenkel emission over the complete voltage range. The higher values of capacitance are achieved at lower frequencies, which is due to the excess capacitance from the interface states in equilibrium with the n-GaN that could respond to the applied ac signal. Noticed that the conductance shows nearly constant value at 10^3–10^5 Hz, and then, the conductance suddenly rises with rising frequency for various applied voltages. The interface state densities (2.32×10^{12} eV^{-1} cm^{-2} at E_C-0.23 eV to 2.38×10^{12} eV^{-1} cm^{-2} at E_C-0.73 eV) and relaxation times (2.85×10^{-5} s at E_C-0.23 eV and 9.21×10^{-4} s at E_C-0.73 eV) are extracted for the Au/Fe_3O_4/n-GaN HJ by using *C*–*f* and *G*–*f* characteristics. The obtained results suggested that the Fe_3O_4 interlayer may be useful candidate for the development of metal/interlayer/semiconductors (MIS) device applications.

Funding Uma is highly grateful to Department of Science and Technology (DST), New Delhi, for providing financial assistance in the form of DST-INSPIRE FELLOWSHIP to purse PhD program. This work was also supported by the National Research Foundation of Korea (NRF) funded by the Ministry of Science, ICT and Fusion Research (2018R1D1A1B07040603) and BK21 Plus funded by the Ministry of Education (21A20131600011).

Compliance with ethical standards

Conflict of interest The authors declare that they have no conflict of interest.

References

1. Siva Pratap Reddy M, Park WS, Im KS et al (2018) Dual-surface modification of AlGaN/GaN HEMTs using TMAH and piranha solutions for enhancing current and 1/f-noise characteristics. J Electron Dev Soc 6:791–796
2. Glavin NR, Chetak KD, Heller ER et al (2017) Flexible gallium nitride for high-performance, strainable radio-frequency devices. Adv Mater 29:1701838
3. Beschoten B, Halperin EJ, Young DK et al (2001) Spin coherence and dephasing in GaN. Phys Rev B 63:121202
4. Bub JH, Rudolph J, Natali F et al (2010) Temperature dependence of electron spin relaxation in bulk GaN. Phys Rev B 81:155216

5. Saha D, Siddiqui L, Bhattacharya P et al (2008) Electrically driven spin dynamics of paramagnetic impurities. Phys Rev Lett 100:196603
6. Saha D, Basu D et al (2010) High-frequency dynamics of spin-polarized carriers and photons in a laser. Phys Rev B 82:205309
7. Krishanmurthy S, Van Schilfgaarde M et al (2003) Spin lifetimes of electrons injected into GaAs and GaN. Appl Phys Lett 83(9):1761–1763
8. Pearton SJ, Abernathy CR, Thaler GT et al (2004) Wide bandgap GaN-based semiconductors for spintronics. J Phys Condens Matter 16:R209–R245
9. Van Erve OMJ, Kioseoglou G, Hanbicki AT et al (2004) Comparison of Fe/Schottky and Fe/Al_2O_3 tunnel barrier contacts for electrical spin injection into GaAs. Appl Phys Lett 84:4334–4336
10. Garrido SF, Ubben KU, Herfort J et al (2012) Electrical characterization of all-epitaxial Fe/GaN(0001) Schottky tunnel contacts. Appl Phys Lett 101:032404
11. Kumar A, Nagarajan S, Sopanen M et al (2015) Temperature dependent 1/f noise characteristics of the Fe/GaN ferromagnetic Schottky barrier diode. Semicond Sci Technol 30:105022
12. Janardhanam V, Jyothi I, Sekhar Reddy PR et al (2018) Double Gaussian barrier distribution of permalloy ($Ni_{0.8}Fe_{0.2}$) Schottky contacts to n-type GaN. Superlattices Microstruct 120:508–516
13. Yang K, Kim DH et al (2011) Schottky barrier effect on the electrical properties of Fe_3O_4/ZnO and Fe_3O_4/Nb: $SrTiO_3$ heterostructures. J Phys D Appl Phys 44:355301
14. Zhang Z, Satpathy S (1991) Electron states, magnetism, and the Verwey transition in magnetite. Phys Rev B 44:13319–13331
15. Coey JMD, Venkatesan M (2002) Half-metallic ferromagnetism: example of CrO_2 (invited). J Appl Phys 91:8345–8350
16. Coey JMD, Versluijs JJ, Venkatesan M (2002) Half-metallic oxide point contacts. J Phys D 35:2457–2466
17. Sun S (2006) Recent advances in chemical synthesis, self-assembly, and applications of FePt nanoparticles. Adv Mater 18:393–403
18. Neuberger T, Schopf B, Hofmann H et al (2005) Superparamagnetic nanoparticles for biomedical applications: possibilities and limitations of a new drug delivery system. J Magn Magn Mater 293:483–496
19. Portet D, Denizot B, Rump E et al (2001) Nonpolymeric coatings of iron oxide colloids for biological use as magnetic resonance imaging contrast agents. J Colloid Interface Sci 238:37–42
20. Meng X, Li H, Chen J et al (2009) Mossbauer study of cobalt ferrite nanocrystals substituted with rare-earth Y^{3+} ions. J Magn Magn Mater 321:1155–1158
21. Zi Z, Sun Y, Zhu X et al (2009) Synthesis and magnetic properties of $CoFe_2O_4$ ferrite nanoparticles. J Magn Magn Mater 321:1251–1255
22. Phua LX, Xu F, Ma YG et al (2009) Structure and magnetic characterizations of cobalt ferrite films prepared by spray pyrolysis. Thin Solid Films 517:5858–5861
23. Bibes M, Villegas JE, Barthelemy A (2011) Ultrathin oxide films and interfaces for electronics and spintronics. Adv Phys 60:5–84
24. Sze SM (1981) Physics of semiconductor devices, 2nd edn. Wiley, New York
25. Rhoderick EH, Williams RH (1988) Metal–semiconductor contacts. Clarendon Press, Oxford
26. Padma R, Sreenu K, Rajagopal Reddy V (2017) Electrical and frequency dependence characteristics of Ti/polyethylene oxide (PEO)/p-type InP organic-inorganic Schottky junction. J Alloys Compd 695:2587–2596
27. Sharma BL (1984) Metal–semiconductor Schottky barrier junctions and their applications. Plenum Press, New York
28. Maril E, Kaya A, Kocyigit S et al (2015) On the analysis of the leakage current in Au/$Ca_3Co_4Ga_{0.001}O_x$/n-Si structure in the temperature range of 80–340 K. Mater Sci Semicond Proc 31:256–261
29. Werner JH, Guttler HH (1991) Barrier inhomogeneities at Schottky contacts. J Appl Phys 69:1522–1533
30. Caldıran Z, Deniz DR, Sahin Y, Metin O, Meral K, Aydogan S (2013) The electrical characteristics of the Fe_3O_4/Si junctions. J Alloys Compd 552:437–442
31. Deniz AR, Caldiran Z, Sahin Y, Sinoforoglu M, Metin O, Meral K, Aydogan S (2013) The synthesis of the Fe_3O_4 nanoparticles and the analysis of the current–voltage measurements on Au/Fe_3O_4/p-Si Schottky contacts in a wide temperature range. Metall Mater Trans A 44A:3811–3814
32. Rajagopal Reddy V, Janardhanam V, Won Jonghan, Choi C-J (2017) Microstructural, electrical and frequency-dependent properties of Au/p-Cu_2ZnSnS_4/n-GaN heterojunction. J Colloid Interface Sci 499:180–188
33. Venkata Prasad C, Siva Pratap Reddy M, Rajagopal Reddy V, Park Chinho (2018) Effect of annealing on chemical, structural and electrical properties of Au/Gd_2O_3/n-GaN heterostructure with a high-k rare-earth oxide interlayer. Appl Surf Sci 427:670–677
34. Rajagopal Reddy V, Venkata Prasad C (2018) Surface chemical states, electrical and carrier transport properties of Au/ZrO_2/n-GaN MIS junction with a high-k ZrO_2 as an insulating layer. Mater Sci Eng B 231:74–80
35. Card HC, Rhoderick EH (1971) Studies of tunnel MOS diodes I. Interface effects in silicon Schottky diodes. J Phys D 4:1589–1601
36. Riad AS (1999) Influence of dioxygen and annealing process on the transport properties of nickel phthalocyanine Schottky-barrier devices. Physica B 270:148–156
37. Reddy MSP, Lee JH, Jang JS (2014) Electrical characteristics of TMAH-surface treated Ni/Au/Al_2O_3/GaN MIS Schottky structures. Electron Mater Lett 10(2):411–416
38. Varghese AC, Menon CS (2005) Electrical properties of hybrid phthalocyanines thin films using gold and lead electrodes. Eur Phys J B 47:485–489
39. Jani O, Ferguson I, Honsberg C et al (2007) Design and characterization of GaN/InGaN solar cells. Appl Phys Lett 91:132117
40. Shao ZG, Chen DJ, Liu B et al (2011) Current transport mechanisms of InGaN metal–insulator–semiconductor photodetectors. J Vac Sci Technol B 29:051201
41. Arslan E, Butun S, Safak Y et al (2010) Investigation of trap states in AlInN/AlN/GaN heterostructures by frequency-dependent admittance analysis. J Electron Mater 39(12):2681–2686
42. Nicollian EH, Goetzberger A (1967) The Si-$Si0_2$ interface-electrical properties as determined by the metal–insulator–silicon conductance technique. Bell Syst Tech J 46:1055–1133
43. Cakar M, Turut A, Onganer Y (2002) The conductance-and capacitance–frequency characteristics of the rectifying junctions formed by sublimation of organic pyronine-B on p-type silicon. J Solid State Chem 168:169–174
44. Duman S, Gurulak B, Dogan S et al (2011) Capacitance and conductance–frequency characteristics of Au-Sb/p-GaSe: Gd Schottky barrier diode. Vaccum 85:798–801
45. Aydogan S, Saglam M, Turut A (2012) Effect of temperature on the capacitance–frequency and conductance–voltage characteristics of polyaniline/p-Si/Al MIS device at high frequencies. Microelectron Reliab 52:1362–1366
46. Chattopadhyay P, Raychaudhuri B (1993) Frequency dependence of forward capacitance–voltage characteristics of Schottky barrier diodes. Solid State Electron 36(4):605–610
47. Nicollian EH, Brews JR (1982) MOS physics and technology. Wiley, New York
48. Singh A (1985) Characterization of interface states at Ni/n-CdF_2 Schottky barrier type diodes and the effect of CdF_2 surface preparation. Solid State Electron 28(3):223–232
49. Cova P, Singh A, Medina A et al (1998) Effect of doping on the forward current transport mechanisms in a

metal–insulator–semiconductor contact to InP: Zn grown by metal organic vapor phase epitaxy. Solid State Electron 42(4):477–485
50. Bati B, Nuhoglu C, Saglam M et al (2000) On the forward bias excess capacitance at intimate and MIS Schottky barrier diodes with perfect or imperfect ohmic back contact. Phys Scr 61:209–212
51. Bulbul MM, Altindal S, Parlakturk F et al (2010) The density of interface states and their relaxation times in $Au/Bi_4Ti_3O_{12}/SiO_2$/n-Si (MFIS) structure. Surf Interface Anal 43:1561–1565
52. Erdogan IY, Gullu O (2010) Silicon MIS diodes with Cr_2O_3 nanofilm: optical, morphological/structural and electronic transport properties. Appl Surf Sci 256:4185–4191
53. Rajagopal Reddy V, Sekhar Reddy PR, Neelakanta Reddy I, Choi C-J (2016) Microstructural, electrical and carrier transport properties of Au/NiO/n-GaN heterojunction with a nickel oxide interlayer. RSC Adv 6:105761–105770
54. Venkata Prasad C, Rajagopal Reddy V, Choi C-J (2017) Electrical and carrier transport properties of the Au/Y_2O_3/n-GaN metal–insulator–semiconductor (MIS) diode with rare-earth oxide interlayer. Appl Phys A 123:279–288
55. Manjunath V, Rajagopal Reddy V, Sekhar Reddy PR, Janardhanam V, Choi C-J (2017) Electrical and frequency-dependent properties of Au/Sm_2O_3/n-GaN MIS junction with a high-k rare-earth Sm_2O_3 as interlayer. Curr Appl Phys 17:980–988

Publisher's Note Springer Nature remains neutral with regard to jurisdictional claims in published maps and institutional affiliations.